Appl. Phys. B 70 [Suppl.], S109–S117 (2000) / Digital Object Identifier (DOI) 10.1007/s003400000362

Applied Physics B
Lasers
and Optics

The criterion of pulse reconstruction quality based on Wigner representation

S. Yeremenko, A. Baltuška, M.S. Pshenichnikov*, D.A. Wiersma

Ultrafast Laser and Spectroscopy Laboratory, University of Groningen, Nijenborgh 4, 9747AG Groningen, The Netherlands

Received: 7 October 1999/Revised version: 21 April 2000/Published online: 24 May 2000 –

Abstract. We propose a new criterion for the assessment of ultrashort pulse reconstruction quality. Our idea is based on the use of a two-dimensional Wigner representation of the electric field. This allows introducing a single measure to represent the quality of both phase and amplitude retrieval. The new criterion is employed to examine two contemporary pulse characterization techniques: FROG (Frequency Resolved Optical Gating) and SPIDER (Spectral Interferometry for Direct Electric-field Reconstruction). For SPIDER, the influence of reference pulse stretching on the quality of phase extraction is investigated. Next, we ascertain the limitations in the use of a Fabri-Perrot etalon in the SPIDER apparatus for producing delayed pulse replicas. For the FROG technique we examine the impact of the doubling crystal orientation on the quality of the amplitude-phase retrieval of sub-5-fs pulses. The introduced criterion is also applied to study the respective sensitivity of FROG and SPIDER to the limited phase-matching bandwidth of the non-linear medium and detector noise.

PACS: 42.30.Rx

Modern applications of ultrashort laser pulses require reliable knowledge of their amplitude and phase [1–5]. Among several techniques that provide access to phase-amplitude information, frequency resolved optical gating (FROG) [6–9] and spectral phase interferometry for direct electric-field reconstruction (SPIDER) [10–13] are the most advanced nowadays. Both methods have a number of distinguished features that determine their applicability under certain experimental conditions. For instance, the main advantage of FROG is that it utilizes excite-probe geometry, common in most nonlinear spectroscopic applications. Therefore, it is ideally suited to characterize pulses precisely at the sample position by simply interchanging the latter with a nonlinear medium for optical gating [14]. On the other hand, SPIDER has the advantage of real-time pulse measurement at high repetition rates [15, 16] since its phase-recovery algorithm involves only a couple of Fourier-transformations [11]. This becomes invaluable in experiments in which the outcome crucially depends on whether each individual pulse meets the preset requirements.

Although ideally both methods allow the precise amplitude-phase retrieval of an ultrashort pulse, in practice specific experimental conditions such as phase-matching, geometry, detector noise, etc., affect the reconstruction quality. This particularly concerns phase information, since in any type of pulse-characterization experiment only the spectral intensity can be measured directly, from which spectral phase extraction follows. Therefore, to assess the correctness of pulse parameter retrieval, one needs a criterion that monitors the quality of pulse reconstruction. Besides the optimization of reconstruction methods, the criterion should also be useful for relative comparison of different techniques.

Several such criteria have been proposed to date [17]. First of all, the *rms* error between temporal intensities of ideal and reconstructed pulses can be employed as a measure of the retrieval quality of pulse shape. However, pulses with different spectral amplitudes and phases may have identical temporal profiles. Hence, the *rms* intensity error can not suffice alone and should be complemented by phase information. The problem with the latter is that a simple *rms* phase error is inappropriate, since the retrieved phase is poorly defined for low-intensity components where it usually exhibits large but meaningless variations. To avoid substantial distortions of the *rms* phase error, an intensity-weighted phase *rms* error has been suggested [17, 18]. Therefore, two different criteria, one for the pulse amplitude and the other for the pulse phase should be used simultaneously.

In this paper we introduce a new, general criterion based on Wigner representation [19] of ultrashort pulses. The criterion embraces both phase and amplitude information in a mixed time-frequency domain, has a high validity, and incorporates a number of aspects of the previously used criteria. Based on the proposed criterion, we examine the limitations and optimal conditions of two pulse-reconstruction techniques that utilize the second-order nonlinearity: SPIDER and second harmonic generation (SHG) FROG. We also compare the techniques on the basis of their sensitivity to the limited phase-matching bandwidth and detector noise. The results illustrate the strength of the criterion in the assessment of the pulse reconstruction quality.

*Corresponding author.
(Fax: +31-50/363-4441, E-mail: M.S.Pshenichnikov@chem.rug.nl)

The paper is organized as follows: in Sect. 1 the criterion of the reconstruction quality based on Wigner representation of ultrashort pulses is introduced. In Sects. 2 and 3 we implement this criterion to optimize SPIDER and SHG FROG techniques. The relative comparison of these two methods from the viewpoint of phase matching and signal/noise ratio is presented in Sect. 4. Finally, in Sect. 5 we summarize our findings.

1 The Wigner representation and the Wigner trace error

The Wigner representation of an ultrashort pulse, $W(t,\omega)$ is straightforwardly calculated from the (complex) electric field in frequency, $E(\omega)$:

$$W(t,\omega)=\int E^*\left(\omega+\frac{\omega'}{2}\right)E\left(\omega-\frac{\omega'}{2}\right)\exp(-i\omega' t)\mathrm{d}\omega' \quad (1)$$

or time domain, $\tilde{E}(t)$:

$$W(t,\omega)=\int \tilde{E}^*\left(t+\frac{t'}{2}\right)\tilde{E}\left(t-\frac{t'}{2}\right)\exp(-i\omega t')\mathrm{d}t' \quad (2)$$

Equations (1) and (2) show that the Wigner trace is a two-dimensional distribution in the time-frequency domain and therefore takes into account both temporal and spectral properties of light pulses. It has been introduced using the analogy of ultrashort light pulses and quantum particles moving in a combined position-momentum phase space [20, 21]. The Wigner distribution was used in pulse-characterization methods [22, 23] and recently, it has also been applied for the interpretation of coherent optical spectroscopy such as photon and Raman echoes [24–26].

An example of a Wigner trace of a pulse with the Gaussian spectrum and cubic spectral phase is shown in Fig. 1a. As follows from (1), integration of $W(t,\omega)$ with respect to time provides the pulse spectrum (Fig. 1b). Subsequently, integration of $W(t,\omega)$ over frequency yields the temporal pulse intensity (Fig. 1c). The Wigner representation is quite intuitive since the shape of the contour (Fig. 1a) generally follows the group delay, i.e. the first derivative of the spectral phase with respect to frequency. Beside this intuitiveness, the Wigner trace contains a delicate balance between the amount of phase and amplitude information. While an element of a Wigner trace is scaled by the respective pulse intensity, its precise location in the time-frequency domain is fully determined by phase information.

As a criterion to judge the pulse-reconstruction quality, we propose a normalized error between Wigner matrices $W^0(t,\omega)$ and $W(t,\omega)$ of ideal and retrieved pulses, respectively:

$$\varepsilon=\sqrt{\sum_{i,j}^{N}\left[W^0_{i,j}(t_i,\omega_j)-\alpha W_{i,j}(T_i,\omega_j)\right]^2}\Bigg/\sqrt{\sum_{i,j}^{N}\left[W^0_{i,j}(t_i,\omega_j)\right]^2}, \quad (3)$$

where α is a scaling factor and N is the size of the matrix. The value ε as given by (3) will be called the *Wigner trace error*. The precise lateral overlap of the two Wigner traces in the time space is required to correctly compute ε due to uncertainty of the absolute pulse position in time. This can be easily arranged by optimizing the respective overlap of temporal marginals. Note that the scaling factor α is chosen in such a way that the Wigner trace error is minimized. Alternatively, one can require the equality of energies (i.e. double integrals of the Wigner matrices over time and frequency) of the ideal and reconstructed pulses. Indeed, the particular choice of normalization does not affect the interpretation of the calculated Wigner trace error.

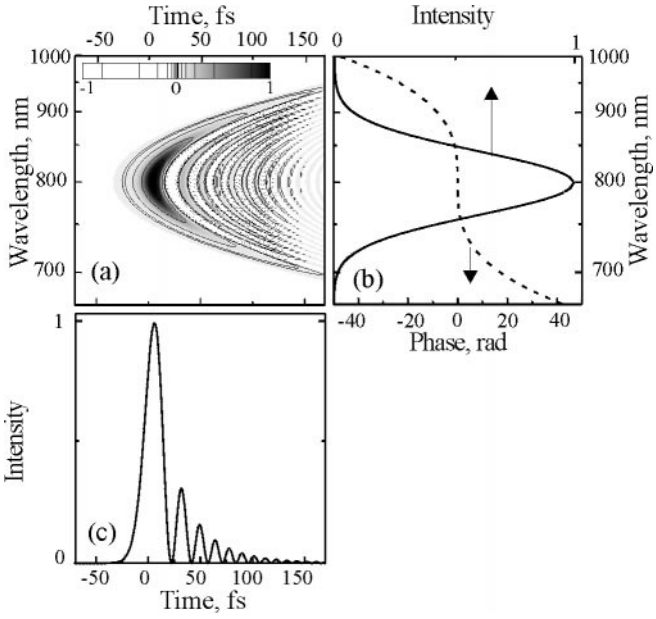

Fig. 1a–c. Wigner representation of a Gaussian pulse with cubic spectral phase (**a**). The corresponding intensity and phase in the frequency and time domains are shown in **b** and **c**, respectively. *Dotted contour lines* in **a** represent negative values

The Wigner trace error ε takes values from 0 to 1, the upper limit being the worst case, in which the difference between the two matrices equals the value of the initial matrix itself. A valuable property of ε is its insensitivity to the matrix size N and to the sampling along the time and frequency axes. From extensive numerical simulations on different pulses we concluded that Wigner trace error below $0.1-0.15$ represents acceptable reconstruction quality.

Together with the introduced criterion based on Wigner representation, it is possible to consider other similar two-dimensional distributions both in the time and frequency domains, for instance, the FROG trace [27]. However, the latter criterion is less sensitive, due to the fact that FROG relies on non-linear frequency conversion and, therefore, a contribution at a given delay and frequency from a weaker spectral component can be hidden beneath the pile-up of contributions from more intense spectral components.

2 Optimization of the SPIDER technique

SPIDER is a relatively new method, which can be regarded as a version of the self-referencing interferometry with spectral shearing [28]. In SPIDER the spectral phase is reconstructed

from a spectral interferogram produced by two replicas of the pulse to be characterized. Two replicas are identical but their carrier frequencies are shifted with respect to each other. In practice, this is accomplished via nonlinear frequency mixing of the delayed replicas with a highly chirped reference pulse that is also derived from the same input pulse. Together with the independently measured spectrum, the spectral phase retrieved from the interferogram is sufficient for the complete characterization of the pulse. In this Section we show how, based on the Wigner trace error, the SPIDER technique can be optimized for the best reconstruction quality.

The SPIDER interferogram, i.e. the signal that is measured in the experiment, has the form

$$I_{SPIDER}(\Omega) = |E_{UP}(\Omega, -\tau) + E_{UP}(\Omega, \tau)|^2 \ . \tag{4}$$

In (4), the electric field of up-converted pulses in the pair $E_{UP}(\Omega, \pm\tau)$ can be calculated in the frequency domain similarly to second harmonic generation [14]:

$$E_{UP}(\Omega, \tau) \propto \int d\omega E(\omega) E(\Omega - \omega) \times \exp\left[i\frac{\omega\tau}{2} + i\varphi_{\text{ref}}(\Omega - \omega)\right] \tag{5}$$

where $E(\omega)$ is the complex spectral amplitude of the pulse to be characterized, τ is the delay between two replicas of the input pulse, and φ_{ref} denotes the additional phase introduced by a stretcher into the reference pulse (that is another replica of the input pulse). We assumed that the intensities of the two pulses that form the interferogram (4) are equal and that the stretcher does not modify the spectrum of the reference pulse. The spectral phase $\varphi(\omega)$ of the input pulse can be derived from the interferogram using a simple algorithm [11].

The intrinsic property of SPIDER is that the quality of phase retrieval depends on the degree of stretching of the reference pulse. It is required that the frequency of the reference pulse does not change appreciably over the duration of the pulse to be characterized. If the reference pulse has been stretched insufficiently, the up-converted pulse (5) acquires an additional spectral phase. Clearly, the stretching factor needed depends on the duration of the pulse to be measured: the longer the input pulse, the longer the reference pulse should be.

To evaluate the influence of the reference pulse length on the quality of phase reconstruction we numerically generated a SPIDER interferogram according to (4) and (5) and then performed the phase reconstruction as described in [11]. Briefly, we Fourier-transform the interferogram into the time domain and filter out the peak centered around time τ, thus discarding the other two peaks around 0 and $-\tau$. Then we perform the Fourier transformation back to the frequency domain and subtract the $\Omega\tau$ term from the obtained phase. The last step concatenates the spectral phase difference.

The stretching of the reference pulse was adjusted by changing the amount of quadratic spectral phase: $\varphi_{\text{ref}}(\omega) \propto \omega^2$. As an input pulse, we have chosen the one presented in Fig. 1. The delay τ was tuned within 400 fs–1 ps in order to maintain the spectral shearing $\Omega_0 \cong 150$–$250\ \text{cm}^{-1}$ that exceeds the Nyquist limit by a factor of 2. Such a value keeps the error caused by the rough sampling of the phase negligibly small. Besides, we used a quadratic approximation of the spectral phase between the nodes (separated by Ω_0). The results of modeling are summarized in Fig. 2a where the Wigner error is depicted as a function of reference pulse duration. The quality of the reconstruction rapidly deteriorates as the reference pulse shortens. For instance, the Wigner trace error approaches the upper acceptable limit of 0.15 when the duration of the reference pulse amounts to ~ 2.5 ps. The reason for the poorer reconstruction quality is found in the transference from the reference pulse quadratic phase, which begins to overwhelm the initial cubic phase of the characterized pulse. Note that in this case the duration of the reference pulse should be longer than the duration of the input pulse at least by a factor of 100 to obtain a reasonable reconstruction quality. This point is illustrated in Fig. 2b, where the Wigner error is shown as a function of the width of the intensity autocorrelation of the input pulse. The reference pulse was stretched to 3.5 ps, while the duration of the input pulse was varied by changing the size of the cubic phase. Figure 2b shows that the quality of the phase reconstruction decreases almost exponentially with the growth of the autocorrelation width.

Based on the analysis of the Wigner trace error, we conclude that the quality of phase reconstruction depends strongly on the reference pulse stretching. One should pay special attention to this, particularly in the case of pulses with high order phase distortions when the FWHM pulse or autocorrelation widths poorly reflect the actual extent of the pulse.

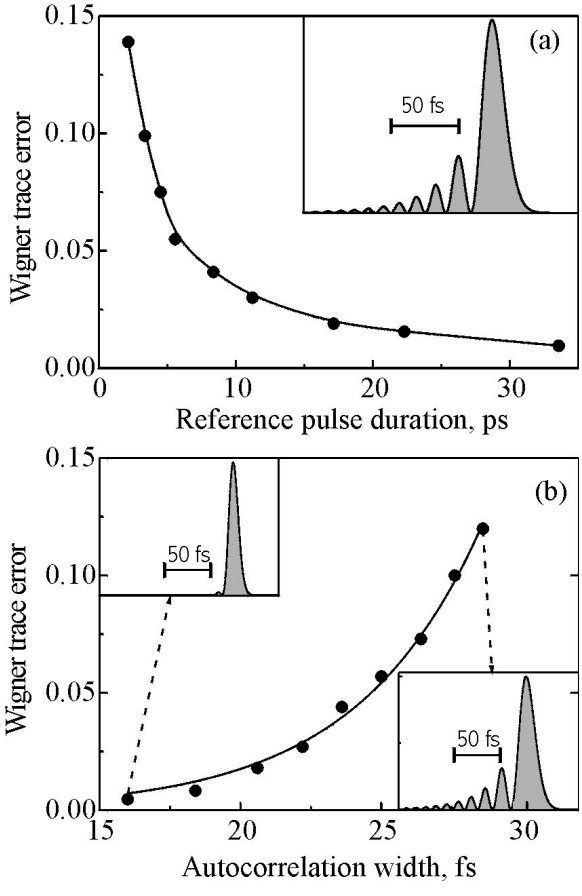

Fig. 2a,b. The influence of the reference pulse length (**a**) and the width of the test pulse intensity autocorrelation (**b**) on the quality of phase reconstruction in SPIDER. The *inset* in **a** gives the temporal intensity profile of the test pulse. The reference pulse in **b** has a 3.5-ps duration. The *insets* in **b** show test pulses belonging to the limiting cases

Another issue of concern in the SPIDER technique is the way to produce two delayed replicas of the input pulse, since the reconstruction algorithm relies on the fact that their spectral phases should be identical. For instance, for characterization of 6-fs pulses, a balanced Mach–Zander interferometer had to be employed [12]. For longer pulses, reflection from a Fabri–Pérrot etalon was suggested [11]. As the etalon, a thin uncoated parallel optical flat can be used. The advantages of the latter are simplicity and low sensitivity to environmental perturbations. However, the pulse replicas, produced by such an etalon, are not entirely identical because one of the pulses passes twice through the material of the etalon while the other does not. The phase difference between the up-converted pulses that forms the SPIDER interferogram has an additional contribution due to material dispersion:

$$\Delta\varphi(\omega) = \varphi(\omega + \Omega_0) - \varphi(\omega) - \varphi^{et}(\omega) \tag{6}$$

where $\varphi(\omega)$ is the spectral phase to be found and $\varphi^{et}(\omega)$ is the additional phase introduced by the etalon. Therefore, the additional phase difference in (6) should be removed before concatenation is performed. For instance, one can calibrate the etalon using conventional interferometry or simply calculate the phase from known dispersion of the material.

Figure 3 illustrates the influence of the etalon dispersion on the quality of phase retrieval in the SPIDER technique when the standard calibration procedure based on the second-harmonic signal [11] is used. We assumed that a spectral limited pulse with the central frequency at 800 nm is reflected off a 75-μm thick etalon made of BK7 glass. Therefore, one of the pulse replicas additionally passed through about 150 μm of glass. The separation between the two pulses introduced by the etalon is about 750 fs. Clearly, for the 75-μm thick etalon the 10-fs pulses can be measured with a satisfactory accuracy without any need for the phase compensation (Fig. 3). However, the Wigner trace error for shorter pulses becomes unacceptably high. Therefore, for pulses shorter than 10 fs the aforementioned methods of etalon calibration should be used. Alternatively, one can employ other means of pulse replicas generation, like the balanced Mach–Zander interferometer.

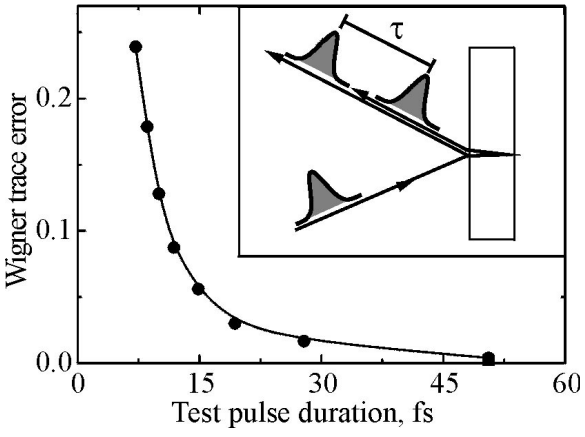

Fig. 3. The reconstruction quality of SPIDER in the etalon arrangement. The *solid circles* correspond to the calculation without any phase compensation while the *squares* represent the case when the third-order phase is introduced to precompensate for the material dispersion in the etalon. The etalon is an uncoated, 75-μm thick optical flat made of BK7 glass

3 FROG optimization

SHG FROG technique is based on the measurements of spectrally dispersed autocorrelation signal [8]:

$$S_{ideal}(\Omega, \tau) = \left| \int E(\omega) E(\Omega - \omega) \exp(-i\omega\tau) \mathrm{d}\omega \right|^2 . \tag{7}$$

The FROG trace is then used as an input to a numerical algorithm that retrieves the intensity and the phase of the pulse. However, the experimentally collected data deviate from the ideal FROG trace as given by (7). In particular, the effect of the limited phase-matching bandwidth of the non-linear medium becomes increasingly important for sub-10-fs pulses [29]. In this Section we analyze two different approaches to selection of a nonlinear crystal for the SHG FROG measurements of 5-fs pulses that have been recently suggested [14, 30, 31].

The complete SHG FROG signal has the form [14, 30]:

$$S(\Omega, \tau) \propto \Omega^2 \left| \int E(\omega) E(\Omega - \omega)\, \mathrm{e}^{-i\omega\tau + i\Delta k(\Omega,\omega)L/2} \times \mathrm{sinc}\left[i\Delta k(\Omega, \omega)L/2\right] \mathrm{d}\omega \right|^2 \tag{8}$$

where τ denotes the delay between pulses, $\Delta k(\Omega, \omega)$ is the phase mismatch

$$\Delta k(\Omega, \omega) = k_0(\omega) + k_0(\Omega - \omega) - k_e(\Omega) \tag{9}$$

and L is the thickness of the doubling crystal. Here we consider Type I phase-matching and neglect the effect of beam geometry and dispersion of the second-order non-linearity. Equation (8) can be simplified to a product of an ideal, i.e. perfectly phase-matched, SHG FROG and a spectral filter [14, 29, 31]:

$$S(\Omega, \tau) \propto R(\Omega) S_{ideal}(\Omega, \tau) \tag{10}$$

where the expression for the spectral filter is given by:

$$R(\Omega) = \Omega^2 \,\mathrm{sinc}^2 \left[\frac{\Delta k(\Omega) L}{2} \right] . \tag{11}$$

The transition from (8) to (10) and (11) involves the expansion of wave vectors $k_0(\omega)$ and $k_0(\Omega - \omega)$ into Taylor series up to the first order. There are two main approaches to such an expansion. The first one [14, 29, 30] is to perform the expansion around frequency $\omega = \Omega/2$, keeping the terms that are linear with frequency. In this case we obtain the following expression

$$\Delta k(\Omega) \approx 2k_0(\Omega/2) - k_e(\Omega) \tag{12}$$

in which the first-order terms containing first-order derivatives cancel each other. In the second approach [31, 32], the wave vectors are expanded around the central frequency of the fundamental pulse ω_0:

$$\Delta k' \approx 2k_0(\omega_0) - k_e(\omega_0) + (\Omega - 2\omega_0) \times \left[\frac{\partial k_0(\omega_0)}{\partial \omega} - \frac{\partial k_e(2\omega_0)}{\partial \omega} \right] . \tag{13}$$

Note that in this case the first derivative terms do not cancel each other and therefore must be retained. The approximate expressions (13) or (14) can be used for finding the orientation angle of the doubling crystal that provides the most suitable spectral filter.

Two distinctly different recommendations on the phase-matching wavelength of the crystal have been suggested based on (12) (called from now on Recipe I) and (13) (Recipe II). Recipe I requires the phase-matching wavelength to be shifted from the central to a higher frequency to ensure adequate up-conversion of the blue wing of the spectrum (Fig. 4a, dashed curve). Subsequently, the FROG trace must be corrected for the frequency-doubling efficiency $R(\Omega)$ that is appreciably important in the IR region due to the Ω^2-factor in (11) (Fig. 4a, solid curve). In contrast, from (13) Recipe II recommends the use of an IR-shifted phase-matching wavelength. In this case, the red wing of the up-conversion spectral efficiency (Fig. 4b, dashed curve) supposedly balances off the Ω^2 term in (11), which results in a nearly symmetric contour around the central wavelength of the pulse (Fig. 4b, solid curve). Because of its large spectral width, it would seem that no additional correction of the FROG trace is needed.

To test the implications of the two recipes and to verify the better approximation of the phase mismatch, we simulated FROG measurements of a 4.5-fs pulse centered at 790 nm. In order to follow a realistic scenario, we modeled the spectrum by a super-Gaussian contour with the bandwidth that supports 4 fs pulses (Fig. 5a). We next assume that the pulse is not perfectly compressed, and a small amount of quartic spectral phase (cubic group delay) broadens the pulse to ~ 4.5 fs. The chosen spectrum is a simplification of a typical fiber output [33] while phase distortions approximately correspond to the residual phase of a compressor consisting of a combination of prisms and chirped mirrors [34]. The Wigner representation of the test pulse is shown in Fig. 5b.

We computed the FROG traces according to (8) for a 10-μm BBO crystal cut for the central wavelength of 700 nm (Recipe I) and 970 nm (Recipe II). Since (8) is exact, no approximations about the phase mismatch are made in these calculations. Next, the first FROG trace was corrected for the spectral filter as given by (11), in agreement with Recipe I. Following Recipe II no correction was applied to the second data set. Both FROG traces were then processed by commercially available software (Femtosoft Technologies) to reconstruct the initial pulse. The error of the FROG retrieval procedure was acceptable in both cases and did not exceed 0.01% (Recipe I), and 0.2% (Recipe II) for a 256×256 FROG matrix. The results of the reconstruction along with the respective Wigner traces are presented in Fig. 5c,d (Recipe I) and Fig. 5e,f (Recipe II). The temporal amplitude and phase of the initial pulse are also shown by solid curves for comparison.

The Wigner error of the reconstructed pulse amounts to merely 0.035 for Recipe I, while for Recipe II the error is as high as 0.24. Indeed, the Wigner trace of the recovered pulse in the case of Recipe I (Fig. 5d) is nearly identical to the input one (Fig. 5b). Consequently, the quality of pulse retrieval is excellent for both amplitude and phase (Fig. 5c). In contrast, the result produced by Recipe II exhibits an entirely different behavior (Fig. 5e,f). The pulse reconstruction has an unacceptably poor quality (Fig. 5e) which is also reflected in considerable discrepancy in the spectral marginal [29, 35]. The inspection of Wigner traces in Figs. 5b and 5f conspicuously shows difference in instantaneous frequency spectra

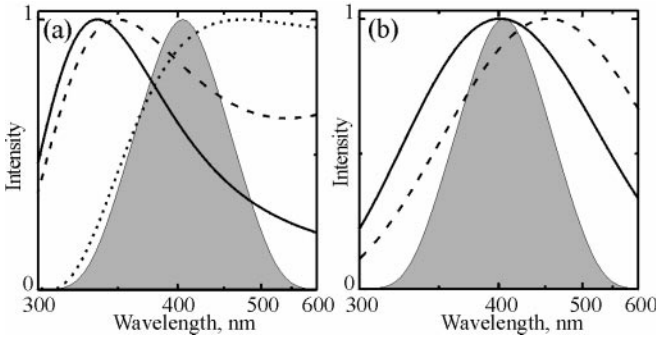

Fig. 4a,b. Spectral filtering effect in the SHG FROG technique for Recipe I (**a**) and Recipe II (**b**). For details see text. The *shaded contour* shows autoconvolution of super-Gaussian intensity spectrum supporting a 4-fs pulse. *Solid* and *dashed curves* represent the total spectral filter $R(\Omega)$ and a sinc^2 term, respectively, calculated according (12) (**a**) and (13) (**b**) for the central wavelength of 700 nm (**a**), and 970 nm (**b**). The thickness of the BBO crystal is 10 μm. *Dotted line* in **a** shows the phase-matching curve calculated according to (12) for the central wavelength at 970 nm

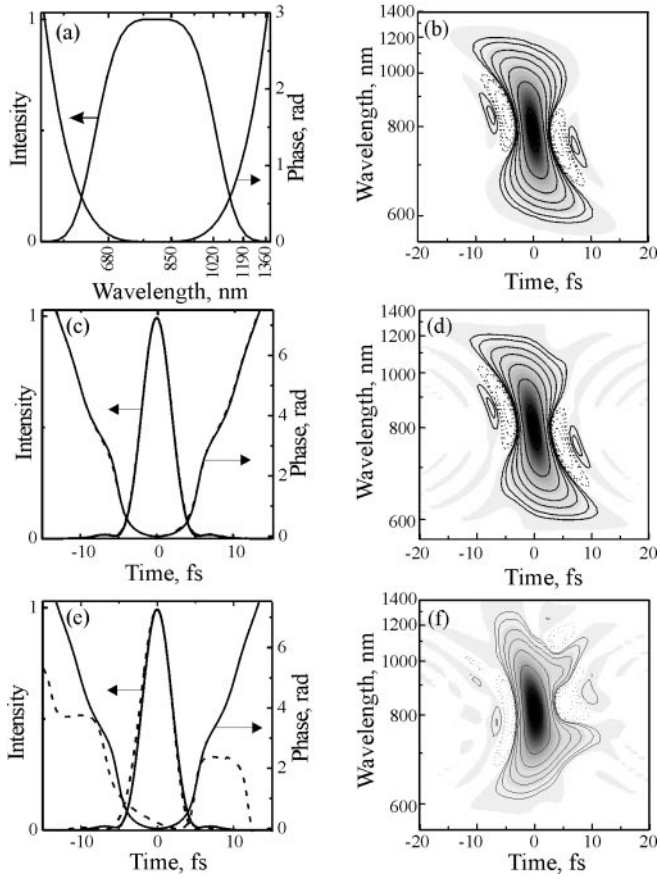

Fig. 5a–f. The comparison of SHG FROG recovery of a 4.5-fs pulse for Recipe I and Recipe II. The spectrum and phase of the input pulse is depicted in **a** with the relevant Wigner distribution hown in **b**. The retrieved pulses according to Recipe I and Recipe II spectrum and phase (*dashed curves*) along with Wigner distributions are presented in **c**,**d** and **e**,**f**, respectively. *Solid curves* in **c** and **e** show the parameters of the input pulse. The convention on *contour lines* in **b**, **d**, and **f** is identical to Fig. 1

of the two pulses, especially at times below and above the half-width of the pulse. Apparently, the intensity of frequency components belonging to the spectral wings is not substantial enough to affect significantly the FWHM pulse duration. On the other hand, such intensities are still usable for a variety of spectroscopic applications [36]. Therefore, misjudgement of the phase distortions can lead to the erroneous interpretation of experimental data.

Now we address the question why Recipe I is superior to Recipe II. The reason lies in the Taylor expansion of the phase mismatch. Recipe I is based on (12) in which zero-order terms are functions of second-harmonic frequency. In contrast, the frequency dependence in (13) is purely quadratic (Fig. 4b, dashed curve). However, crystal dispersion is low in the infrared and rapidly increases as the UV absorption is approached [37]. Equation (13) fails to capture this feature while (12) correctly predicts the high-frequency slope of the phase-matching curve to be steeper than the low-frequency one (Fig. 4a, dashed curve). Therefore, tuning the central wavelength of the crystal to a longer wavelength, as Recipe II recommends, does not allow correction of the FROG trace for the imposed spectral filter since the conversion efficiency becomes extremely low in the blue wing (Fig. 4a, dotted curve). This should be compared to Recipe I in which the correction is readily applied (Fig. 4a, solid curve). Hence, for FROG characterization of ultrashort pulses one should consider a crystal with the phase-matching wavelength blue-shifted with respect to the central frequency, as suggested by Recipe I.

4 Relative comparison of SHG FROG and SPIDER techniques

In this Section we analyze the comparative performance of SHG FROG and SPIDER methods of pulse reconstruction. Using the Wigner trace error as a criterion, we consider the stability of these techniques in face of the finite spectral bandwidth of a nonlinear crystal and detector noise.

4.1 Thickness of the nonlinear crystal

To evaluate the effect of phase matching in the nonlinear crystal on the retrieval quality, we calculated a SPIDER interferogram and FROG trace according to (4), (5) and (8), respectively. However, (5) should be generalized to include the finite thickness of the crystal:

$$E_{UP}(\Omega,\tau) \propto \Omega \int \mathrm{d}\omega E(\omega)E(\Omega-\omega)\,\mathrm{sinc}\left(\frac{\Delta k(\Omega,\omega)L}{2}\right) \times \exp\left[i\frac{\omega\tau}{2}+i\varphi_{\mathrm{ref}}(\Omega-\omega)-i\frac{\Delta k(\Omega,\omega)L}{2}\right]. \quad (14)$$

Equations (8) and (14) illustrate the different role of the nonlinear crystal in FROG and SPIDER: the former method is based on the *second harmonic* generation while the latter one uses frequency *up-convertion*. For the FROG technique the group velocities of the pulse replicas should be identical, and, hence, the use of Type I phase matching is quite essential [14]. In contrast, SPIDER does not have such a limitation since frequency mixing occurs between two different pulses. Therefore, Type II phase matching can be used in order to broaden the spectral acceptance bandwidth.

In our model calculations, we considered Type I of phase matching for FROG and both Type I and Type II for the SPIDER technique. The orientation of the BBO crystal was chosen as $\theta = 29^\circ$ for Type I and $\theta = 42^\circ$ for Type II that corresponds to the maximal efficiency at the central wavelength of the pulse (800 nm). As a test pulse we used the pulse presented in Fig. 1. The phase from the SPIDER interferogram and the amplitude and phase from the FROG trace were extracted using the algorithms described above.

The results of the pulse reconstruction quality for different crystal lengths are presented in Fig. 6 for FROG and Fig. 7 for SPIDER. Both techniques have quite similar sensitivities to the crystal thickness when Type I of phase matching is used (solid circles in Figs. 6 and 7). For instance, for the acceptable Wigner trace error of ~ 0.15, an ~ 30-μm BBO crystal should be used. However, the use of Type II phase matching in the SPIDER technique allows lengthening the crystal up to 50-μm (solid squares in Fig. 7).

As we discussed in Sect. 3, the correction for the spectral filter in SHG FROG relaxes the requirements on the crystal length and allows using much longer nonlinear crystals. In the same way, a similar correction can be introduced in SPIDER. To do so, (14) is simplified to a product of an ideal, i.e. a perfectly phase-matched part and a spectral filter:

$$E_{UP}(\Omega,\tau) \propto \Omega\,\mathrm{sinc}\left(\frac{\Delta k(\Omega)L}{2}\right)\exp\left(-i\frac{\Delta k(\Omega)L}{2}\right) \times E^{UP}_{ideal}(\Omega) \quad (15)$$

where $E^{UP}_{ideal}(\Omega,\tau)$ is given by (5), $\Delta k(\Omega)$ is given by (12) for Type I phase-matching and

$$\Delta k(\Omega) \approx k_0(\Omega/2) + k_e(\Omega/2) - k_e(\Omega) \quad (16)$$

for Type II phase-matching. Equation (16) is derived similarly to (12) with the only difference that the first derivative terms do not cancel each other out and have been disregarded.

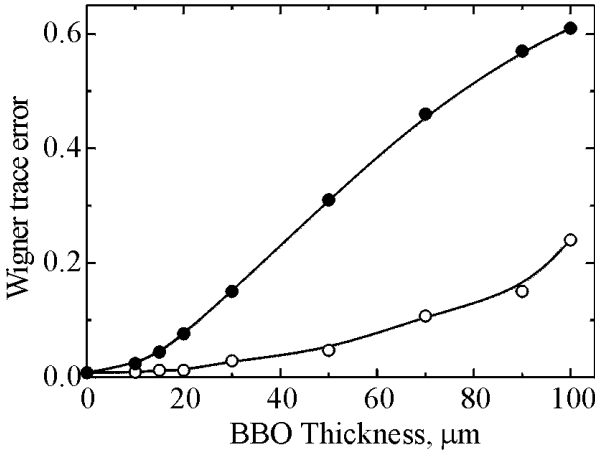

Fig. 6. The dependence of the reconstruction quality of SHG FROG method on the thickness of the nonlinear crystal. *Solid* and *open symbols* correspond to the calculation without and with spectral correction, respectively

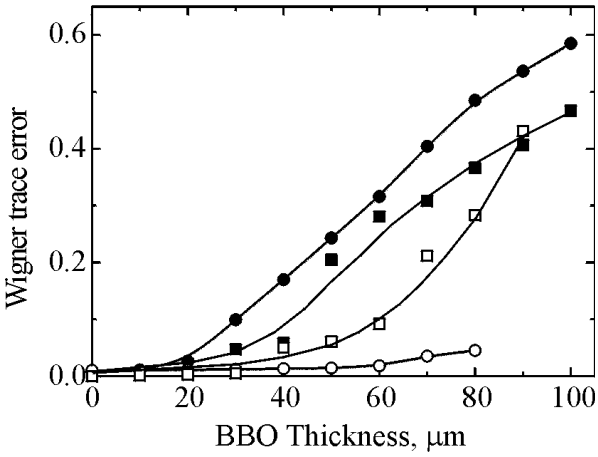

Fig. 7. The dependence of the reconstruction quality of SPIDER method on the thickness of the nonlinear crystal for the Type I (*circles*) and Type II (*squares*) of the phase-matching. *Solid* and *open symbols* correspond to the calculation without and with spectral correction, respectively

The results of the calculations with the spectral correction for FROG are presented in Fig. 6 (open symbols) and for SPIDER in Fig. 7 (open circles for Type I of the phase matching and open squares for Type II). First of all, the correction allows choosing a much thicker crystal in both SHG FROG and SPIDER techniques. Secondly, the correction in the case of Type I phase matching in SPIDER gives much better results than in the case of Type II phase-matching because (16) presents a worse approximation than (12). Finally, the calculations show that in the case of Type I of phase matching the correction is more efficient for SPIDER than for FROG. The explanation of this fact lies in the details of pulse reconstruction. In contrast to FROG, where both the spectrum and the phase are retrieved from a single FROG trace, the pulse spectrum in SPIDER is measured independently. Therefore, it is not distorted by up-conversion in the nonlinear crystal. Furthermore, it follows from (15) that the additional phase shift due to the phase mismatch does not depend on the delay between the two replicas and hence the additional phase shift is canceled out in the interferogram (4). Therefore, the only remaining source of error is the value of the spectral shear Ω_0 that is determined as the frequency spacing between the maxima of the up-converted spectra of the two pulse replicas. However, in the case of insufficient bandwidth the up-converted spectra are skewed, which leads to an incorrect estimation of Ω_0. This is immediately reflected in the poor quality of the phase extraction. The correction of the up-converted spectra for the amplitude filter almost entirely removes the error in the value of spectral shear and gives excellent pulse reconstruction. The residual error is due to the narrowing of the spectral region with appreciable intensities where the phase is defined reasonably well.

Our simulations show that the main source of inaccuracy in the SPIDER method lies in the incorrect determination of the spectral shear as the nonlinear crystal distorts shapes of the up-converted spectra. Therefore, under such circumstances one should use different methods to determine the spectral shear. It has been suggested [11] that the delay between pulse replicas can be measured from a conventional interferogram, and the spectral shear is found out from the calculated dispersion of the stretcher. The other method is to calibrate the SPIDER apparatus from the shift of interferograms while the time overlap between the reference pulse and the test pair is changed. We point out that these methods are not free from systematic errors related to either calibration procedure or inaccuracy in the spectral dispersion of the stretcher. Note that FROG does not require as many calibration procedures as SPIDER. Also, FROG frequency and time marginals are powerful tools to verify experimental data [7–9].

4.2 Signal/noise ratio

Next we compare performance of SPIDER and SHG FROG pulse retrieval techniques in the presence of detector noise. The question we are addressing in this Section is: what noise level in SPIDER interferograme and FROG trace is still tolerable for acceptable pulse reconstruction quality? We chose additive noise with a Gaussian distribution and a zero mean value as an example of the noise that occurs in CCD cameras. We considered the cases of ideal phase-matching (zero-thickness nonlinear crystal) described by (4), (5) for SPIDER and (7) for FROG. The stretching of the reference pulse in SPIDER was sufficiently high to minimize the Wigner trace error corresponding to the noiseless reconstruction. As a test pulse we again used the pulse presented in Fig. 1. The noise, with its *rms* amplitude normalized to the maximum value of the signal, was added to numerically generated FROG traces and SPIDER interferograms. Since the pulse spectrum is measured separately in SPIDER, we added to the spectrum the same noise fraction as to the interferogram. The pulse parameters were reconstructed using the algorithms described in previous Sections, and the Wigner trace error was calculated for each noise fraction. The retrieval procedures were applied without any prior filtering of the data sets. However, since noise filtering is implicitly present in the SPIDER algorithm (when the peak centered around time τ is filtered out), the noise fraction was accordingly increased to ensure a fair comparison.

The results of the simulations are presented in Fig. 8. SPIDER and FROG show quite a similar stability to the ad-

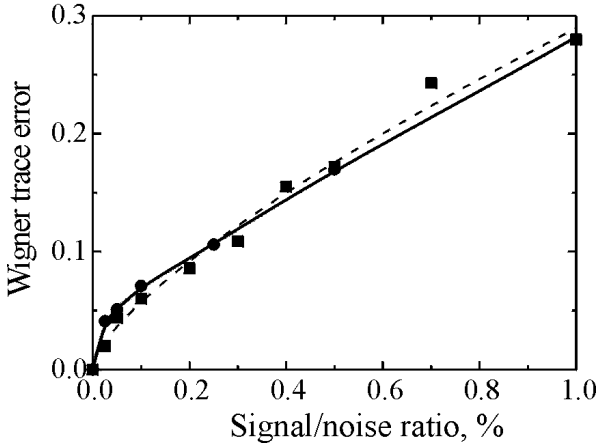

Fig. 8. The reconstruction quality of SPIDER (*circles, solid curve*) and FROG (*squares, dashed curve*) as a function of signal/noise ratio

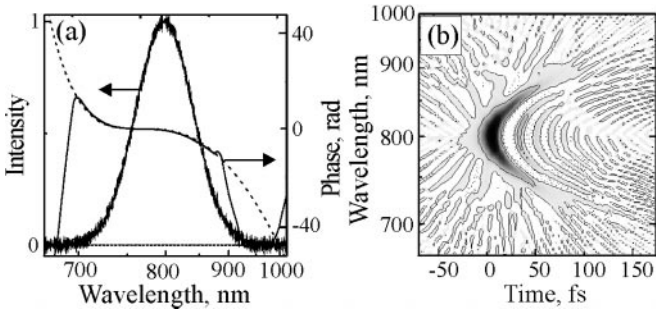

Fig. 9a,b. The results of SPIDER retrieval in the case of 1% additive noise. The spectrum and the reconstructed spectral phase are shown in **a** by *solid curves*, while a *dashed line* represents the spectral phase of the test pulse. Wigner representation of the retrieved pulse is depicted in **b**

ditive noise. The *rms* noise level of approximately 0.5% can be considered as the upper limit when both algorithms give acceptable reconstruction quality. It is well known [17] that the performance of FROG can be dramatically improved by a prior filtering of the measured trace. The same argument can be applied to SPIDER as well. Particular noise-filtering strategy depends on pulse peculiarities since it is coupled with the danger of wiping out essential information.

Figure 9a presents an example of the pulse retrieved by the SPIDER technique in the case of 1-% additive noise. The relevant Wigner representation, depicted in Fig. 9b, should be compared with the Wigner representation of the initial pulse (Fig. 1a). The plots clearly demonstrate that the main source of the error is due to substantial phase distortions in areas where the spectral intensity is low and the relative fraction of the noise increases.

So far, we have considered the case of equal *rms* amplitudes of the additive noise in the SHG FROG trace and SPIDER interferogram. However, the SPIDER interferogram is a one-dimensional data set while the FROG trace is a two-dimensional one. Hence, during the measurement of a single $n \times n$ FROG trace one can collect n SPIDER interferograms obtaining a considerably lower noise level. For instance, for a typical dimension of the FROG matrix of 128×128 elements this yields a better by a factor of $\sqrt{128}$ signal-noise ratio. From the other hand, FROG utilizes second-harmonic generation while SPIDER uses up-conversion that requires a substantial (by at least a factor of 100, see Sect. 3) stretching of the reference pulse. As a result, intensities of the up-converted replicas are 100 times weaker than those of second harmonics. Therefore, with a given noise level of the photodetector, SPIDER in general requires an order of magnitude more intense input pulse than FROG.

Up to now equal intensities of pulse replicas in both FROG and SPIDER were assumed. This situation, however, is not always realized in an experiment. The difference in the replica intensities leads to the decrease of modulation depth in the SPIDER interferogram thus causing deterioration of the phase retrieval quality in the presence of noise. The same argument can be applied to SHG FROG where the second harmonic intensity is the highest if the initial pulse is split into two identical replicas. Our simulations show that, in the case of uneven replica intensities and given camera noise, the relative performance of both techniques remains similar to that depicted in Fig. 8.

5 Conclusions

The new way of assessing the reconstruction quality of ultrashort pulses, introduced in this paper, fills in the deficit of a single measure accounting for both amplitude and phase recovery provided by various ultrashort pulse measuring techniques. Since the Wigner trace error is based on the comparison of two two-dimensional distributions that uniquely describe a complex electric field of the laser pulse, the proposed criterion has an extremely high validity. Unlike numerous existing amplitude and phase errors that are computed either in the time or frequency domain, the proposed criterion aptly grasps the role of subtle amplitude-phase deviations, to which, for instance, the temporal intensity profile remains largely insensitive. Furthermore, this criterion is supplemented by an intuitive and comprehensive graphic representation (Wigner trace) that is very useful for understanding the character of the pulse distortions.

We have employed this criterion to study the performance of two techniques that utilize second harmonic generation: SHG FROG and SPIDER. In the case of SPIDER we have quantitatively analyzed the influence of the reference pulse stretching to the quality of phase reconstruction. Analysis of the Wigner trace errors has revealed that insufficient stretching of the reference pulse leads to essential distortions of the recovered phase, especially in the case of the pulses with the higher than second order of the spectral phase. The correct amount of the reference pulse stretching should be established with respect to the measured pulse's longest temporal feature. The latter, especially in the case of a complicated spectral intensity and/or phase pattern, can considerably exceed the temporal FWHM. We have also shown the limitations in the use of a Fabri–Perrot etalon for producing the delayed pulse replicas. Our numerical simulations also prove that the use of an etalon in the SPIDER apparatus leads to the erroneous interpretation of the retrieved data in the case of the broadband laser spectra that support the pulse duration of 10 fs and shorter.

In the analysis of the FROG technique, the distortions of the amplitude-phase measurements of sub-5-fs pulses have been examined, which arise from different orientations of a doubling crystal. It has been shown that the proper angular tuning of the crystal and the correction of the FROG trace for the spectral filter can significantly reduce the problems of the limited phase-matching bandwidth.

The SPIDER and SHG FROG techniques have been compared among themselves under similar conditions with respect to their sensitivity to the limited phase bandwidth. Spectral corrections have been introduced to minimize the effect of spectral filtering that is a direct result of the finite SHG crystal thickness. The need for such a correction appears to be more important for FROG than for SPIDER because for the truthful pulse retrieval the former method requires the correct intensity of the second harmonic signal, while the latter technique draws phase-sensitive information from interference fringes filling the intensity envelope. Therefore, the narrowing of the up-conversion bandwidth in SPIDER results in a smaller spectral interval on which the phase of the measured pulse is recovered. The correction of individually up-converted spectra in SPIDER is, nonetheless, very important in order to recover the right amount of spectral shearing. Our simulations have convincingly shown that spectral fil-

tering in the SHG crystal is responsible for a shift of the individual second- harmonic spectra of the two pulse replicas with respect to each other. This shift appears as a sizable addition to the true value of the spectral shearing. The failure to account for this contribution compromises the subsequent use of concatenation routine. Finally, the impact of the finite signal/noise ratio has been examined in detail for both SPIDER and SHG FROG. The simulations generally resulted in the similar level of the Wigner trace error for both methods within acceptable limits.

Concluding, we believe that the Wigner trace error, introduced in this paper, will find wide use in optimization and relative comparison of already existing and emerging techniques of full characterization of ultrashort pulses. The strength of the new criterion makes is particularly useful for a quantitative analysis of performance of different pulse measuring methods with respect to the experimental noise, systematic errors, dynamic range, etc. It allows finding the optimal experimental conditions for various cases and also constitutes a benchmark for comparison of different techniques among themselves. An entirely new promising field of application of the proposed criterion can be found in the comparison of results of phase-sensitive ultrafast spectroscopy [38–44] and theoretical models [24].

Acknowledgements. We thank R. Trebino, I. Walmsley, D. Kane, and L. Gallmann for fruitful discussions. We are also grateful to S. Mukamel and M. Joffre for drawing our attention to Wigner representation of ultrashort laser pulses. The investigations were supported by the Netherlands Foundation of Physical Research (FOM) and Chemical Research (SON) with financial aid from the Netherlands Organization for the Advancement of Science (NWO).

References

1. C.J. Bardeen, Q. Wang, C.V. Shank: Phys. Rev. Lett. **75**, 3410 (1995)
2. C.J. Bardeen, J. Che, K.R. Wilson, V.V. Yakovlev, P. Cong, B. Kohler, J.L. Krause, M. Messina: J. Phys. Chem. **101**, 3815 (1997)
3. J. Zhou, J. Peatross, M.M. Murane, H.C. Kapteyn, I.P. Christov: Phys. Rev. Lett. **76**, 752 (1996)
4. V.V. Yakovlev, C.J. Bardeen, J.C.J. Che, K.R. Wilson: J. Chem. Phys. **108**, 2309 (1998)
5. A. Baltuska, Z. Wei, R. Szipöcs, M.S. Pshenichnikov, D.A. Wiersma: Appl. Phys. B **65**, 175 (1997)
6. D.J. Kane, R. Trebino: IEEE J. Quantum Electron. **QE-29**, 571 (1993)
7. R. Trebino, D.J. Kane: J. Opt. Soc. Am. B **10**, 1101 (1993)
8. K.W. DeLong, R. Trebino, J. Hunter, W.E. White: J. Opt. Soc. Am. B **11**, 2206 (1994)
9. R. Trebino, K.W. DeLong, D.N. Fittinghoff, J.N. Sweetser, M.A. Krumbugel, B.A. Richman, D.J. Kane: Rev. Sci. Instrum. **68**, 3277 (1997)
10. C. Iaconis, I.A. Walmsey: Opt. Lett. **23**, 792 (1998)
11. C. Iaconis, I.A. Walmsey: IEEE J. Quantum Electron. **QE-35**, 501 (1999)
12. L. Gallmann, D.H. Sutter, N. Matuschek, G. Steinmeyer, U. Keller, C. Iaconis, I.A. Walmsley: Opt. Lett. **24**, 1314 (1999)
13. C. Dorrer: Opt. Lett. **24**, 1532 (1999)
14. A. Baltuska, M.S. Pshenichnikov, D.A. Wiersma: IEEE J. Quantum Electron. **35**, 459 (1999)
15. I.A. Walmsley, C. Iaconis, T. Shuman, M.E. Anderson, E. Kosik, M. Knox, L. Waxer, J. Bromage: In *Ultrafast Optics* (Monte Verita, Ascona, Switzerland 1999)
16. C. Dorrer, B. d. Beauvoir, C.L. Blanc, S. Ranc, J.-P. Rousseau, P. Rousseau, J.-P. Chambaret, F. Salin: Opt. Lett. **24**, 1644 (1999)
17. D.N. Fittinghoff, K.N. DeLong, R. Trebino, C.L. Ladera: J. Opt. Soc. Am. B **12**, 1955 (1995)
18. D.N. Fittinghoff, K.N. DeLong, R. Trebino, C.L. Ladera: J. Opt. Soc. Am. B **12**, 1955 (1995)
19. Y. Meyer: *Wavelets: Algorithms and Applications* (SIAM, Philadelphia 1993)
20. J. Paye: IEEE J. Quantum Electron. **QE-28**, 2262 (1992)
21. J. Paye, A. Migus: J. Opt. Soc. Am. B **12**, 1480 (1995)
22. M. Beck, M.G. Raymer, I.A. Walmsley, V. Wong: Opt. Lett. **18**, 2041 (1993)
23. I.A. Walmsley, V. Wong: J. Opt. Soc. Am. B **13**, 2453 (1996)
24. S. Mukamel: *Principles of Nonlinear Optical Spectroscopy* (Oxford University Press, New York 1995)
25. S. Mukamel, C. Ciordas-Ciurdariu, V. Khidekel: IEEE J. Quantum Electron. **QE-32**, 1278 (1996)
26. V.M. Akulin, V.A. Dubovitskii, A.M. Dykhne, A.G. Rudavets: In *Femtochemistry*, ed. by M. Chergui (Lausanne, Switzerland 1995) p. 62
27. K.W. DeLong, D.N. Fittinghoff, R. Trebino: IEEE J. Quantum Electron. **QE-32**, 1253 (1996)
28. V. Wong, I.A. Walmsley: Opt. Lett. **19**, 287 (1994)
29. G. Taft, A. Rundquist, M.M. Murnane, I.P. Christov, H.C. Kapteyn, K.W. DeLong, D.F. Fittinghoff, M.A. Krumbuegel, J.N. Sweetser, R. Trebino: IEEE J. Sel. Top. Quantum Electron. **2**, 575 (1996)
30. A. Baltuska, M.S. Pshenichnikov, D.A. Wiersma: Opt. Lett. **23**, 1474 (1998)
31. Z. Cheng, A. Furbach, S. Sartania, M. Lenzner, C. Spielmann, F. Krausz: Opt. Lett. **24**, 247 (1999)
32. A.M. Weiner: IEEE J. Quantum Electron. **QE-19**, 1276 (1983)
33. G.P. Agrawal: *Nonlinear fiber optics*, 2nd ed. (Academic press, San Diego 1995)
34. C. Spielmann, M. Lenzner, F. Krausz, R. Szipocs: Optics **120**, 321 (1995)
35. K.W. DeLong, R. Trebino, D.J. Kane: J. Opt. Soc. Am. B **11**, 1595 (1994)
36. A. Kummrow, M.F. Emde, A. Baltuska, M.S. Pshenichnikov, D.A. Wiersma: J. Phys. Chem. **102**, 4172 (1998)
37. V.G. Dmitriev, G.G. Gurzadyan, D.N. Nikogosyan: *Handbook of Nonlinear Optical Crystals* (Springer-Verlag, Berlin 1991)
38. W.P. de Boeij, M.S. Pshenichnikov, D.A. Wiersma: Chem. Phys. **233**, 278 (1998)
39. M.F. Emde, W.P. de Boeij, M.S. Pshenichnikov, D.A. Wiersma: Opt. Lett. **22**, 1338 (1997)
40. W.P. de Boeij, M.S. Pshenichnikov, D.A. Wiersma: In *Annual Review of Physical Chemistry*, Vol. 49, ed. by H.L. Strauss, G.T. Babcock, S.R. Leone (Palo Alto, CA 1998) pp. 99–123
41. A. Tokmakoff, M.J. Lang, D.S. Larsen, G.R. Fleming: Chem. Phys. Lett. **272**, 48 (1997)
42. O. Buccafusca, X. Chen, W.J. Walecki, A.L. Smirl: J. Opt. Soc. Am. B **15**, 1218 (1998)
43. J.-P. Likforman, M. Joffre, V. Thierry-Mieg: Opt. Lett. **22**, 1104 (1997)
44. S.M. Gallagher, A.W. Albrecht, J.D. Hybl, B.L. Landin, B. Rajaram, D.M. Jonas: J. Opt. Soc. Am. B **15**, 2338 (1998)